Structural Engineering and Mechanics, *Vol. 64, No. 1 (2017) 45-58*
DOI: https://doi.org/10.12989/sem.2017.64.1.045

The influence of convoy loading on the optimized topology of railway bridges

Arne Jansseune* and Wouter De Corte

Department of Structural Engineering, Research group Schoonmeersen, Faculty of Engineering and Architecture, Ghent University, Valentin Vaerwyckweg 1, 9000 Ghent, Belgium

(Received March 11, 2017, Revised June 7, 2017, Accepted July 10, 2017)

Abstract. This paper presents the application of topology optimization as a design tool for a steel railway bridge. The choice of a steel railway bridge is dictated by the particular situation that it is suitable for topology optimization design. On the one hand, the current manufacturing techniques for steel structures (additive manufacturing techniques not included) are highly appropriate for material optimization and weight reduction to improve the overall structural efficiency, improve production efficiency, and reduce costs. On the other hand, the design of a railway bridge, especially at higher speeds, is dominated by minimizing the deformations, this being the basic principle of compliance optimization. However, a classical strategy of topology optimization considers typically only one or a very limited number of load cases, while the design of a steel railway bridge is characterized by relatively concentrated convoy loads, which may be present or absent at any location of the structure. The paper demonstrates the applicability of considering multiple load configurations during topology optimization and proves that a different and better optimal layout is obtained than the one from the classical strategy.

Keywords: topology optimization; SIMP; steel railway bridge; multiple load cases

1. Introduction

Topology optimization is a mathematical approach that seeks to determine the optimum material distribution within a design domain under (mechanical) loads and boundary conditions. The search is driven by objective functions (i.e., the goal) and proceeds iteratively until convergence is achieved and design requirements (i.e., the constraints) are satisfied, resulting in a highly material efficient structure. This method has already been successfully applied in automotive applications, aerospace structures, medicine, and in structural engineering (Stromberg *et al*. 2012, Luo and Kang 2012, Beghini *et al*. 2014), for example in bridge design (Rahmatalla and Swan 2003, Huang and Xie 2008, Fauche *et al*. 2010, Liu and Qiao 2011, Briseghella *et al*. 2013, 2016, Zuo *et al*. 2012, 2014, Kutylowski and Rasiak 2014a, b).

The application of the classical strategy of topology optimization typically considers only one or a very limited number of load cases. For bridge design, this simplification often leads to unrealistic designs. For instance, the optimal geometry for a simply supported rectangular design domain with only a point load in the middle of the lower edge closely resembles half of a bicycle wheel, a result found in many student bridge design contests. Consequently, the presumption is that the classical strategy of topology optimization is not really representative for bridge design and can lead to incorrect optimization. Therefore, this study is devoted to how topology optimization in bridge design deals with multiple load cases. In literature, different examples can be found with multiple load scenarios which demonstrate the importance of considering multiple loads (Bendsøe and Sigmund 2003). For structural engineering applications, only very few studies were conducted recently on optimum topology design for multiple load case problems. A first study proposed a methodology to increase convergence speed and reduce computational cost by calculating the structural compliance as the sum of the strain energies of all elements, but only taking into account the most critical load case in each element (Iwamura and de Faria 2013). Tang *et al*. focused on the application of CFD simulation and topology optimization techniques for the conceptual design of perimeter bracings of high-rise building structures considering multiple wind loads and showed, among other things, the importance to consider multiple load cases with different wind direction (Tang *et al*. 2014).

In this contribution, a study of multi-load topology optimization is presented for a steel railway bridge which carries two tracks and is supported by two lateral main girders, coupled by transverse crossbeams and floorbeams. Because a nominally pinned connection is frequently assumed, between the transverse floorbeams and the lateral main girders, it is sufficient to simplify the main structural system to a 2D design domain. A classical design approach based on influence lines is no longer possible here, since an influence line in addition to parameter (force, deformation, etc.) and location depends on the shape of the layout which continuously changes with the evolution of the layout. In other words, it is impossible to determine one "fixed" most disadvantageous location of a vertical loading. For that reason, a large number of combinations of distributed loads and convoys will be considered as defined in *4. Loading configurations*.

*Corresponding author, Doctor-Assistant
E-mail: Arne.Jansseune@UGent.be

ISSN: 1225-4568 (Print), 1598-6217 (Online)

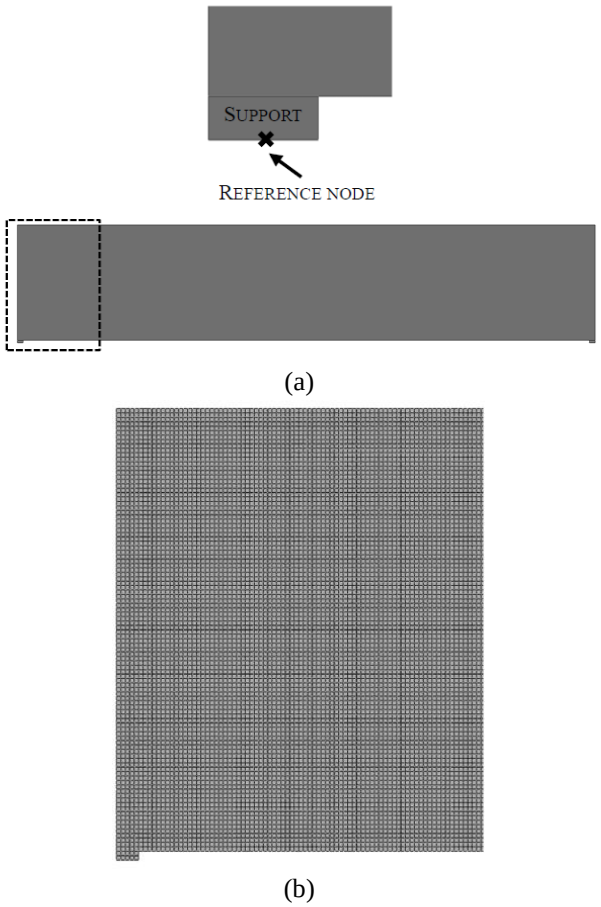

(a)

(b)

Fig. 1 (a) Design domain of the default geometry of the railway bridge; (b) FE model with mesh

Using the topology optimization module in the FE software Abaqus (Simulia 2014a), topology layouts are obtained for bridges with a variable depth to span ratio, with different support conditions, and considering a large number of different load configurations. Depending on these characteristics, a truss frame structure, an arch bridge, or a hybrid structure are obtained. Furthermore and more importantly, the results indicate that it is relevant for topology optimization to perform a multiple load optimization, since a different optimal and better layout is obtained than the one from the classical strategy.

2. Theoretical background

The focus of the current study is on topology optimization to the design of bridges through the application of the Solid Isotropic Material with Penalization (SIMP) method.

2.1 Problem description

To find an optimal material distribution within the design domain, minimization of compliance C was selected as objective function (Eq. (1)) and combined with a volume constraint V^* (Eq. (2)). Since compliance is the inverse indicator of structural stiffness, minimizing the compliance amounts to maximize the stiffness or minimize the deformations. Since the design of a railway bridge is dominated by deformations, especially at high speeds (EN 1993-2 2006), the compliance objective is very relevant to this case study.

$$\text{Minimize} \quad C = \sum^{m} \boldsymbol{u}^T \cdot \boldsymbol{K} \cdot \boldsymbol{u} \tag{1}$$

Where C is the total non-weighted structural compliance or the sum of the strain energy (i.e., energy taken by the structure under the external loads) of all elements and all calculation steps, $\boldsymbol{u}$ is the displacement vector, $\boldsymbol{K}$ is the global stiffness matrix, m is the number of calculation steps. In addition, in finite element analysis, the static equilibrium equation of a structure is expressed as $\boldsymbol{K} \cdot \boldsymbol{u} = \boldsymbol{f}$, in which $\boldsymbol{f}$ is the force vector.

$$\text{Subject to} \quad V^* - \sum_{e=1}^{n} v_e x_e = 0 \ \text{ with } \ 0 \leq \rho \leq 1 \tag{2}$$

Where V^* is the prescribed volume limit for the complete design domain, v_e is the element volume, and x_e is the design variable (here: the material density ρ).

2.2 Material interpolation

In the SIMP formulation, the element stiffness E_i and the element density ρ_i are related through a power-law relationship (Bendsøe 1989, Rozvany and Birker 1994, Yang and Chuang 1994)

$$E_i = E_{min} + \rho_i^p \cdot (E_0 - E_{min}) \tag{3}$$

Where E_0 and E_{min} are the Young's moduli of the solid phase and the void phase respectively, while p denotes the penalization factor. The latter forces the material density ρ towards zero (void) or one (solid) by penalizing regions of intermediate densities (grey zones with $0 < \rho < 1$).

2.3 Optimization strategy

The search to an optimal layout or topology optimization is an iterative process and consists of a number of iterations or design cycles (approximately 30 to 100). Each design cycle starts by updating the design variables (element densities) using an optimization algorithm (Bendsøe and Sigmund 2003), trying to satisfy the objective function (minimize compliance) and constraint (volume). Next, the material properties (element stiffnesses) of the FE model are modified. Then a general static stress/displacement geometric linear analysis is conducted on the modified FE model. Such an analysis consists of one calculation step (one load optimization) or a series of calculation steps (multiple load optimization) because each load configuration considered is applied in a separate calculation step. In this paper, the load cases are discussed in *4. Loading configurations*. Finally, the analysis and optimization results are reviewed to determine whether or not the optimal solution has been reached, by evaluating the objective functions and the constraints. The optimization loop is repeated until convergence is reached or until a stop condition is achieved.

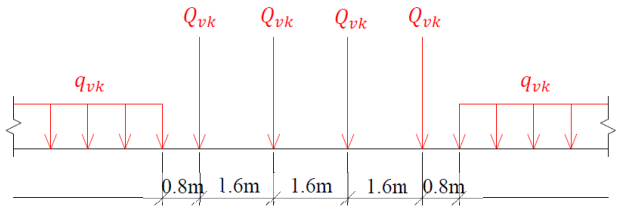

(a) Load Model 71

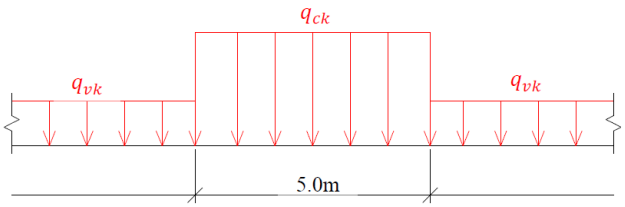

(b) Distributed Load Model 71

Fig. 2 Load Model 71 and characteristic values for vertical loads (EN 1991-2 2003)

3. Numerical model

The numerical investigation was conducted with the commercial finite element program Abaqus (Simulia 2014a) in combination with the optimization software Tosca (Simulia 2014b). The basic steel railway bridge model has a span L of 50 m and a depth D is 10 m ($D/L = 1/5$), while the depth D has been increased from 5 m to 15 m ($1/10 \leq D/L \leq 1/3.33$) in steps of 5m to be able explore the influence of the depth to span ratio D/L. The girder of the railway bridge is modelled as a 2D rectangular design domain and is discretized into 50mm thick quadrilateral S4 shell elements. A default mesh size of 0.10m was adopted, which corresponds to 500 elements in longitudinal direction and 100 elements in vertical direction for the default 50×10 m design domain (See Fig. 1). The material behavior is purely elastic with a Young's modulus $E_0 = 210$ GPa and a Poisson's ratio $\nu = 0.3$. The supports are modelled by rigid bodies which allow for rotation about the reference node (middle of the lower edge) (See Fig. 1) and are not included in the optimization design domain. Three supporting conditions are considered: (i) pinned support and roller support, (ii) two pinned supports, and (iii) one pinned support and two roller supports for a two-span continuous beam.

As already mentioned in *1. Introduction*, the SIMP method was used as provided by the Abaqus software (Simulia 2014a). The objective function or goal of the optimization is to minimize the compliance C, which is adopted in this study as the sum of the strain energy of all elements and all calculation steps (Eq. (1)). The volume constraint V^* is set as 30% of the total volume (Eq. (2)). The default Abaqus settings were used for all other optimization task parameters: a normal density update strategy with a maximum change in density per design cycle of 0.25 and a penalization factor p of 3 (Eq. (3)).

4. Loading configurations

For rail traffic actions, five models of railway loading are defined in (EN 1991-2 2003). From these, the static effect of vertical loading due to normal railway traffic on mainline railways is represented by Load Model 71. This model consists of a vertical uniformly distributed load q_{vk} with a characteristic value of 80 kN/m and four point loads (per rail), representing the locomotive axles, Q_{vk} with a characteristic value of 250kN (See Fig. 2(a)). In this study,

Table 1 Load configurations

	Convoy position	Configuration		Convoy position	Configuration
LG1	-	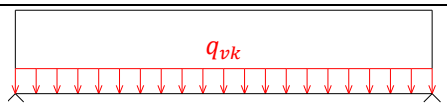	LG2	Start	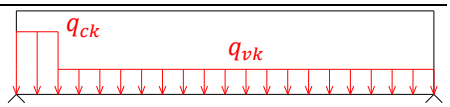
				Middle	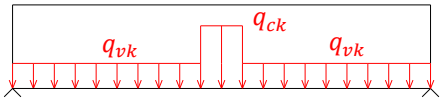
				End	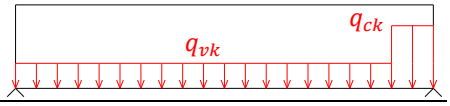
LG3	Start	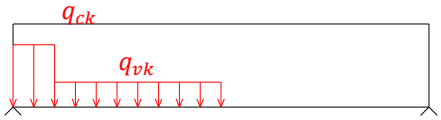	LG4	Start	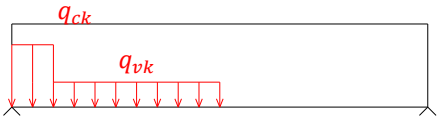
	One fourth	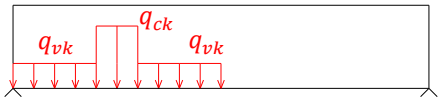		Just before middle	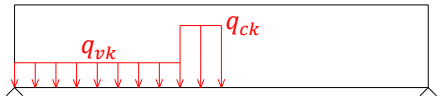
	Middle	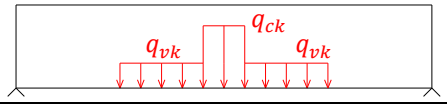		Just after middle	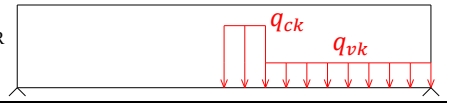

these point loads are transformed into a 5 m long convoy q_{ck} with a characteristic value of 200 kN/m (See Fig. 2(b)). Depending whether any part of this load model is favorable or unfavorable for a given action, it should be applied or removed from the load configuration. Traditionally, this is done based on the appropriate influence line for the action (i.e. moment, shear force, deflection) under consideration, but here replaced by a multiple load case approach.

To explore the influence of one or multiple load optimization, four load groups were defined. These load groups are illustrated in Table 1 and are denoted by LG1 to LG4. Load group LG1 is the simplest one and includes a full load q_{vk} over the full span. The other load groups LG2 to LG4 consist of a 5m long convoy q_{ck} - which moves up in steps of 2.5 m from left to right of the span - and a full load q_{vk} over the other part of the full span (LG2) or of half of the span (LG3 and LG4). For LG3, the center of the full load q_{vk} coincides with and moves up with the center of the convoy, except when the center of the convoy lies in the first or last quarter of the span. In these cases, the full load is applied on the left or right half of the span, respectively (similar to LG4). For LG4, the full load q_{vk} is applied over the same half of the span (the left or right half) as the convoy. In total, this amounts to 57 loading configurations representing all different positions of a moving railway convoy.

The abbreviations of the load groups LG1 and LG4 will be used throughout the text. It is important to mention that, for example, LG2 includes all convoy positions of Table 1, from the most left convoy to the most right convoy and all intermediate positions

In this study, a double track fully loaded bridge is investigated, meaning that the load is equally distributed between both lateral main girders or that the magnitude of the load on one main girder (i.e., the design domain) is equal to that of one track. Although this situation may not represent a frequently occurring load case, it corresponds to the most disadvantageous situation of quasi-static moving trains. Since all loads are applied on the lower edge of the design domain, the lower row of elements are frozen or excluded from the topology optimization.

5. Results

The result section starts with the discussion of the influence of the mesh size and the evolution of the optimal layout of the default model and the influence of the volume fraction for a one load optimization. Next, for two cases the optimal topologies are compared between one and multiple load optimization. Consequently, a parametric study has been conducted using multiple load optimization to investigate the influence of the depth to span ratio and the support conditions. Finally, a two-span bridge is considered. For reasons of clarity, the most important features of the geometry and characteristics of the optimization will be mentioned at the beginning of each subsection.

5.1 One load optimization

The default model is a lateral main bridge girder with a 50 m span and a 10 m depth, which will be further abbreviated as L50-D10. The girder is supported at the bottom by one fixed and one free pinned support. In the first part of this section, the volume fraction V^* is equal to 0.3, while the volume fraction varies in the second part to investigate its influence. For the "one load" optimization, load group 1 or LG1, consisting of a uniform load on the full span, is chosen.

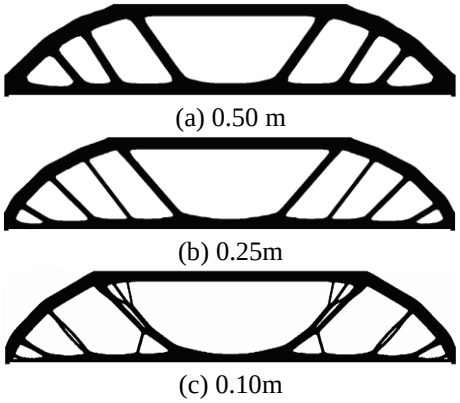

(a) 0.50 m

(b) 0.25m

(c) 0.10m

Fig. 3 Influence of the mesh size on the topology for L50-D10 model (optimized for LG1)

5.1.1 Influence of the mesh size

The mesh size was varied between 0.5 m and 0.1 m. From Fig. 3, it can be seen that seen that the global optimized topology is independent of the mesh size, while the member thickness decreases and the level of detail increases as the mesh is more refined.

5.1.2 Evolution of the topology during optimization

The structural optimization of the default model requires 44 design cycles before the optimal result is found. In Fig. 4(a), the evolution of the compliance C relative to the compliance of the non-optimized design domain with solid material and a thickness equal to 30% of the initial thickness C_{ref} is plotted in black against the iteration number. From this graph, it can be seen that the initial design (with a Young's modulus E_0 of 210 GPa and $V^{*p} \cdot E = 0.29^3 \cdot 210$ GPa=5.28 GPa for the frozen lower edge and the design domain, respectively) has a compliance which is 7.0 times larger than the non-optimized solution with 30% volume fraction. During optimization, the compliance changes rapidly in the beginning and, towards the end more gradually to the solution. The optimal design has a compliance which is 35% smaller than the non-optimized solution. On the same graph, the gray curve represents the dimensionless maximum vertical deflection or the ratio of the maximum vertical deflection δ divided by the maximum deflection of the non-optimized design domain with solid material and a thickness equal to 30% of the initial thickness δ_{ref}. Clearly, and as expected, the maximum deflection and the compliance have the same trend. The optimal design has a maximum deflection which is 26% smaller than the non-optimized solution. Fig. 4(b) shows the evolution of the volume fraction V^* towards 0.3.

To study the evolution of the topology during

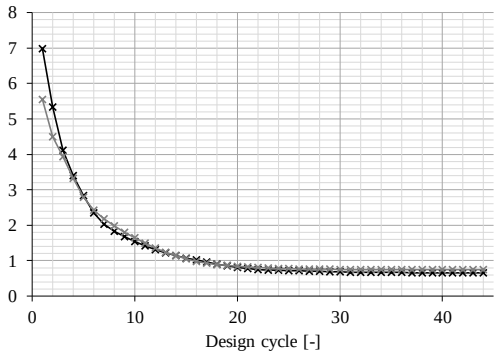

(a) Evolution of the dimensionless compliance C/C_{ref} [-] (black curve) and the dimensionless maximum vertical deflection δ/δ_{ref} [-] (gray curve)

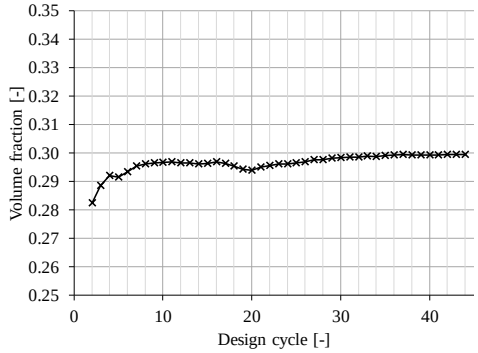

(b) Evolution of the volume fraction V^* [-]

Fig. 4 Evolution of the objective function (a) and the volume constraint (b) for L50-D10 model (optimized for LG1)

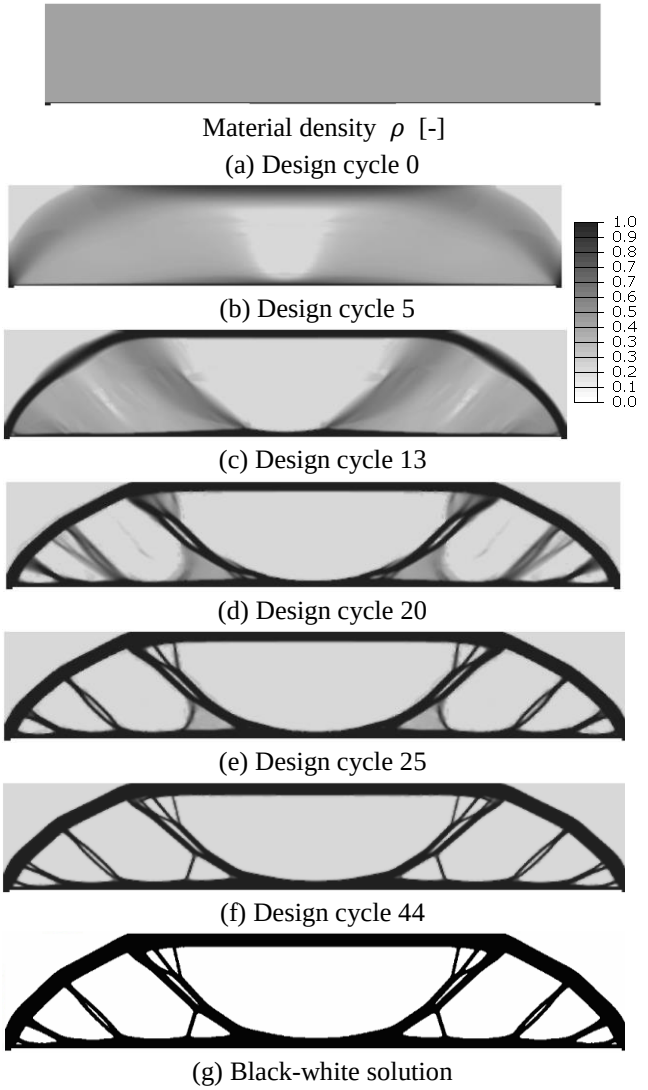

(a) Design cycle 0

(b) Design cycle 5

(c) Design cycle 13

(d) Design cycle 20

(e) Design cycle 25

(f) Design cycle 44

(g) Black-white solution

Fig. 5 Evolution of the material density ρ [-] during topology optimization for L50-D10 model (optimized for LG1)

optimization, the material density ρ is plotted in Fig. 5 at some key moments. Solid ($\rho = 1$) and void ($\rho = 0$) are respectively colored in black and white, while gray regions have an intermediate density ($0 < \rho < 1$) of which the degree of grayness reflects the transition between solid and void. The design domain at the start of the topology optimization is given in Fig. 5(a) and shows that all element densities are initially equal to 0.3 (i.e., the volume fraction V^*), except for the frozen area at the lower edge. By comparing Fig. 5(a) with Fig. 5(b) and (c), the evolution of the layout during the first thirteen cycles can be understood. On the one hand, material is removed in the upper corners and the central area, and these areas also expand; while on the other hand, the creation of an arch between the supports is visible where the material density increases towards one. From cycle 13 (i.e., Fig. 5(c)), a web member in the middle of the span having the appearance of a suspension cable and several inclined web members near the supports resembling hangers start to develop, while the central hole expands further and new openings appear between the hangers.

When all material with a material density ρ smaller than 0.3 is considered as void and is cut from the optimal layout obtained after the last iteration (See Fig. 5(f)), the black and white solution of the topology optimization is obtained as presented in Fig. 5(g). The latter topology is a hybrid between a truss and an arch and is composed of (i) a lower chord which ties the fixed and the free pinned support, (ii) an arch or upper chord connecting the supports, (iii) a web middle of the span, and (iv) several web members resembling inclined hangers near the supports.

To understand the structural behavior of the topology during and after optimization, the maximum in-plane principal stresses are plotted in Fig. 6 at the key moments as in Fig. 5. In these plots, tensile and compressive stresses are, respectively, positive and negative, and colored in red and green. The downward load is acting on the lower chord, transferred to the arch or upper chord via the hangers or web members, and then to the supports via the arch or upper chord. This load transfer generates tension in the lower chord and web members and compression in the upper chord. Because one of the supports permitted to move longitudinally, the compression in the arch is balanced by tension in the tied lower chord. During optimization, both the maximum compressive (arch) and tensile (lower chord) principal stresses decrease by the gradual development of connections (i.e., hangers) between both. The final design has a maximum compressive and tensile principal stress of -

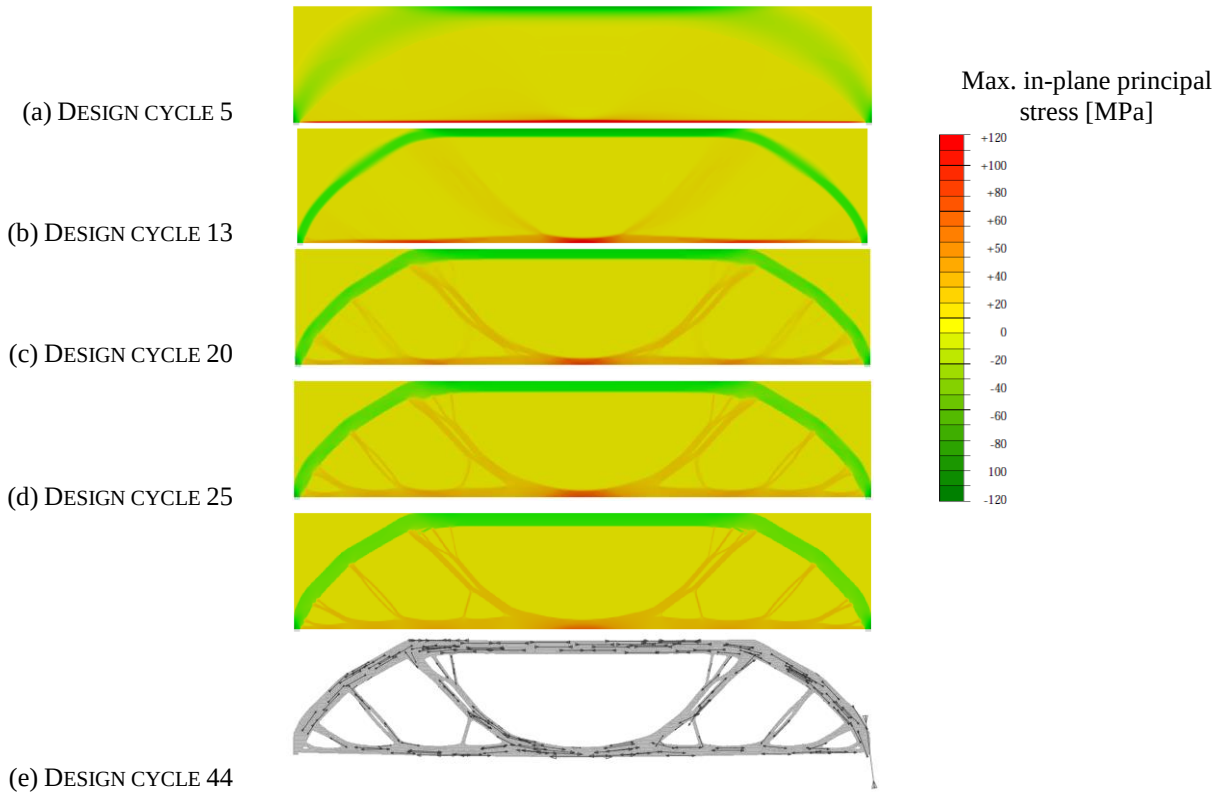

Fig. 6 Evolution of the maximum in-plane principal stresses during optimization for L50-D10 model (optimized for LG1)

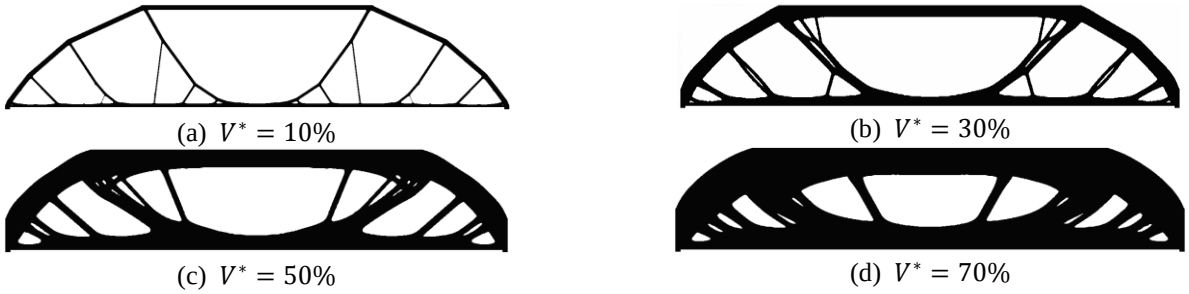

Fig. 7 Topology optimization results for L50-D10 model with different volume fraction V^* (optimized for LG1)

53.4 MPa in the arch and +84.4 MPa in the lower chord, respectively.

5.1.3 Volume fraction

In Fig. 7, the optimum topologies are illustrated for different volume fractions V^*. It appears that the topology and the position of the web members remain relatively similar. The main difference is the thickness of all members as well as the connections. With increasing volume fraction, the additional material is used to increase the thickness and stiffness of all members and to increase the stiffness in the connections, rendering the structure less flexible.

In Fig. 8(a), the maximum deflection δ_{max} relative to the maximum deflection of the initial non-optimized design domain δ_{ref} (with a volume fraction V^* equal to 1.0) is plotted in black against the volume fraction V^*. By halving the volume fraction from 1.0 to 0.5, the maximum deflection increases only 56%. For smaller volume fractions, the maximum deflection is increasing more rapidly than for larger volume fractions. Next, the efficiency of the structure is examined closer, where the most efficient structure is the one with the smallest maximum deflection per unit volume. Therefore, the maximum deflection per unit volume of the optimized domain δ_{max}/V is divided by the maximum deflection per unit volume of the initial non-optimized design δ_{ref}/V_{ref} (or $\delta_{max}/\delta_{ref} \cdot V^*$) is plotted against the volume fraction V^* (See Fig. 8(b)). This graph shows that the non-optimized design domain (with $V^* = 1.0$) is by far the least efficient structure and that the efficiency decreases first rapidly and then slowly as the volume fraction decreases. For this case and for the above definition of efficiency, the most efficient topology has a volume fraction V^* of 0.2 and is independent of the considered deflection limit.

In previous section, the mechanism of topology optimization on the topology, the structural behavior of the optimal topology, as well as the influence of the volume fraction have been clarified for one specific case (L50-D10) using a simple “one load” topology optimization strategy (LG1). The next step is to study the influence of other and

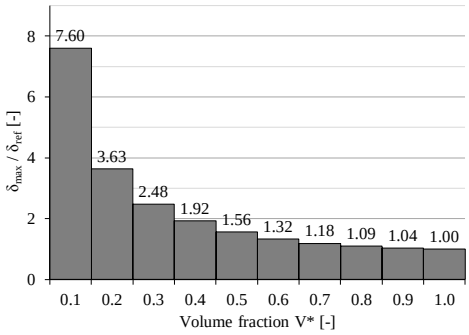

(a) Plot of the dimensionless maximum deflection as a function of the volume fraction

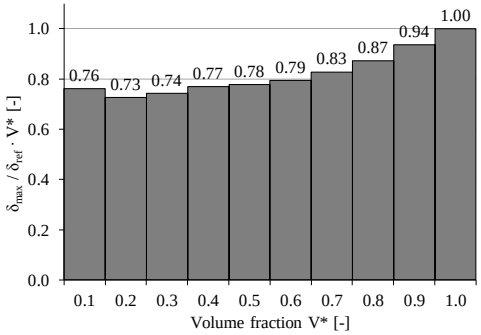

(b) Plot of the dimensionless maximum deflection per volume-unit as a function of the volume fraction

Fig. 8 Influence of the volume fraction on the deformations of the L50-D10 model (optimized for LG1)

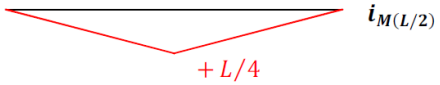

(a) Bending moment in the middle of the span

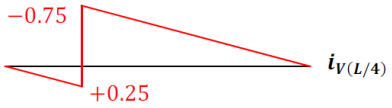

(b) Shear force at one fourth of the span

Fig. 9 Influence lines

multiple loading configurations using a "multiple load" topology optimization strategy.

5.2 One versus multiple load optimization

The first geometry considered is the default bridge girder with a 50 m span and a depth of 10 m (L50-D10) which corresponds to a depth to span ratio D/L of $1/5$. In Fig. 10, the optimized structures are depicted for the different alternatives of topology optimization considering one or multiple load groups LG1 to LG4 (See Table 1). From this figure, it can be seen that the upper chord as well as the lower chord are quite similar in all cases, while the number and the position of the hangers is very different. The latter clearly depends on the load configurations considered during optimization.

As mentioned before, the objective of topology optimization is to minimize the compliance and so the total

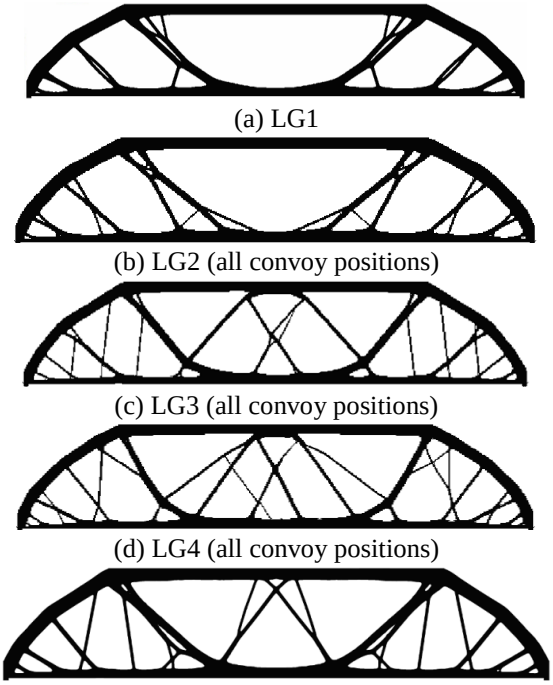

(a) LG1

(b) LG2 (all convoy positions)

(c) LG3 (all convoy positions)

(d) LG4 (all convoy positions)

(e) All load groups and all convoy positions

Fig. 10 Topology optimization results for L50-D10 model optimized for different load groups

deflections δ of the design structure, which are a combination of bending and shear deformations (See Eq. (4)). The bending deformations δ_M depend on the bending moment M and the bending stiffness, which in turn is a function of the Young's modulus E, the area moment of inertia I, the span L, and the boundary conditions (Eq. (4)). Topology optimization can thus only reduce the bending deformations δ_M by increasing the moment of inertia I by adding material in the upper and lower chords where the largest bending moments occur. On the other hand, the shear deformations δ_V depend on the shear force V and the shear stiffness, which in turn is a function of the shear modulus G, the shear area A, and the shape of cross-section (Eq. (4)). To minimize the shear deformations δ_V, topology optimization must primarily add material in the web where the shear force is large. In summary, to accomplish the most efficient material allocation, topology optimization has to find a balance between these two contradicting means: add material in the chords as well as in the web.

$$\delta = \delta_M + \delta_V = \iint \frac{M}{EI} + \iint \frac{V}{GA} \tag{4}$$

From the influence line of the bending moment M in the middle of a simply supported beam (See Fig. 9(a)), it can be seen that load has the largest impact on the bending moment M when it is positioned near the middle of the span. In analogy with a beam under pure bending, the moment of inertia I - and thus the bending stiffness or the resistance against bending deformation - is largely influenced by the (vertical) distance between the upper and lower chord. This reasoning to the reduction of the bending deformations is confirmed by the optimal topology which

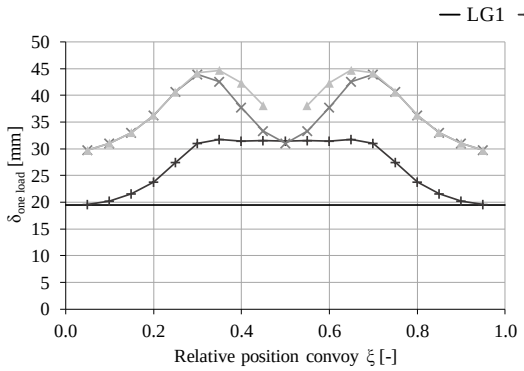

(a) Maximum deflection $\delta_{one\ load}$ [mm] of the one load optimized topology (See Fig. 10 (a))

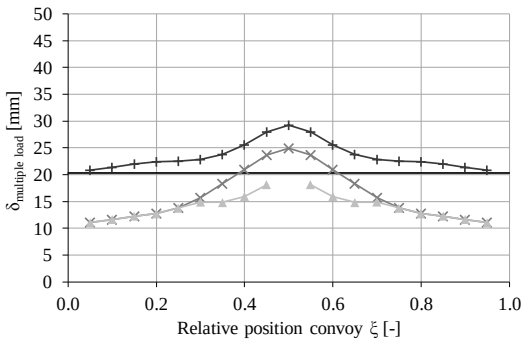

(b) Maximum deflection $\delta_{multiple\ load}$ [mm] of the multiple load optimized topology (See Fig. 10 (e))

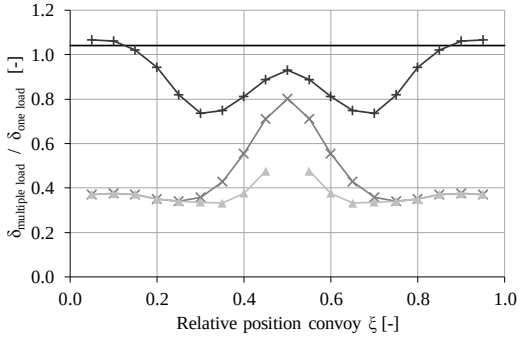

(c) Ratio of the maximum deflections of the multiple load optimized topology to the one load optimized topology $\delta_{multiple\ load}/\delta_{one\ load}$ [-]

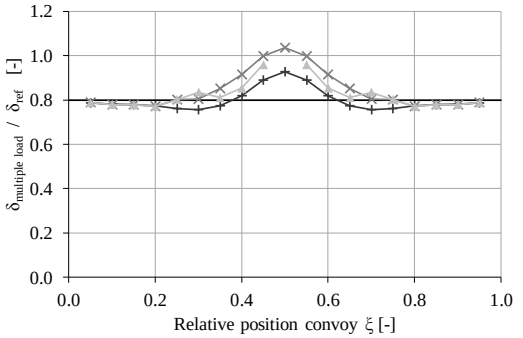

(d) Ratio of the maximum deflections of the multiple load optimized topology to the non-optimized design domain with a thickness equal to 30% of the initial thickness $\delta_{multiple\ load}/\delta_{ref}$ [-]

Fig. 11 Maximum absolute or relative deflections as a function of the relative position of the convoy ξ [-] for the different load groups LG1 to LG4 for L50-D10 model

consists of an upper chord (arch near the supports and horizontal member in the middle section) and lower chord (See Fig. 10).

A similar reasoning can be applied for the shear forces based on influence lines and in analogy with a beam under pure bending. To obtain an as large as possible shear force (near the supports), only a part of the span has to be loaded (such as LG3 and LG4), either the region with a negative influence value or the region with a positive influence value in Fig. 9(b). Irrespective of the load groups considered during optimization, inclined web members can be found near the supports which provide shear resistance and reduce shear deformations (See Fig. 10). By considering a moving convoy together with a partially loaded span (i.e., LG3 and LG4), the layout is during optimization driven to a solution with additional web members in the middle zone to avoid excessive shear deformations in that area (Fig. 10 (c) to (e)). Thus, LG3 and LG4 clearly have a significant impact on the final topology.

To assess whether or not the multiple load optimal topology of Fig. 10(e) is in terms of deformations effectively better than the one load optimal layout of Fig. 10(a), both optimized topologies are subjected to all load groups LG1 to LG4. The maximum deflection $\delta_{one\ load}$ of the one load optimized topology, the maximum deflection $\delta_{multiple\ load}$ of the multiple load optimized topology, and the ratio of these maximum deflections $\delta_{multiple\ load}/\delta_{one\ load}$ are plotted against the relative position of the center of the convoy on the lower edge in Fig. 11(a) to (c), respectively. This parameter ξ ranges from 0.05 for the leftmost convoy to 0.95 for the rightmost convoy in increments of 0.05.

For a uniformly distributed load over the entire span (i.e., LG1), the maximum deflection of the multiple load topology is 4% higher than the maximum deflection of the one load topology. As can be seen in Fig. 12(a), the deformed shapes are very similar, regardless of the difference in topology. In other words, for a uniform load, the multiple load topology is slightly worse than for the one load topology.

When the convoy is situated close to the supports in the case of LG2 ($\xi < 0.12$ or $\xi > 0.88$), the maximum deflection of the multiple load topology is still close to (up to 7% higher than) the maximum deflection of the one load topology. In contrast, for 50 of the 57 load conditions (LG2 with $0.12 < \xi < 0.88$, LG3, and LG4), the maximum deflection of the multiple load topology is (much) smaller than for the one load topology. For the average LG2, LG3, and LG4 convoy, the maximum deflection decreases by 10%, 55%, and 63%, respectively. Furthermore, it is noticeable that the decrease of the maximum deflection largely depends on the position of the convoy. For LG3 for

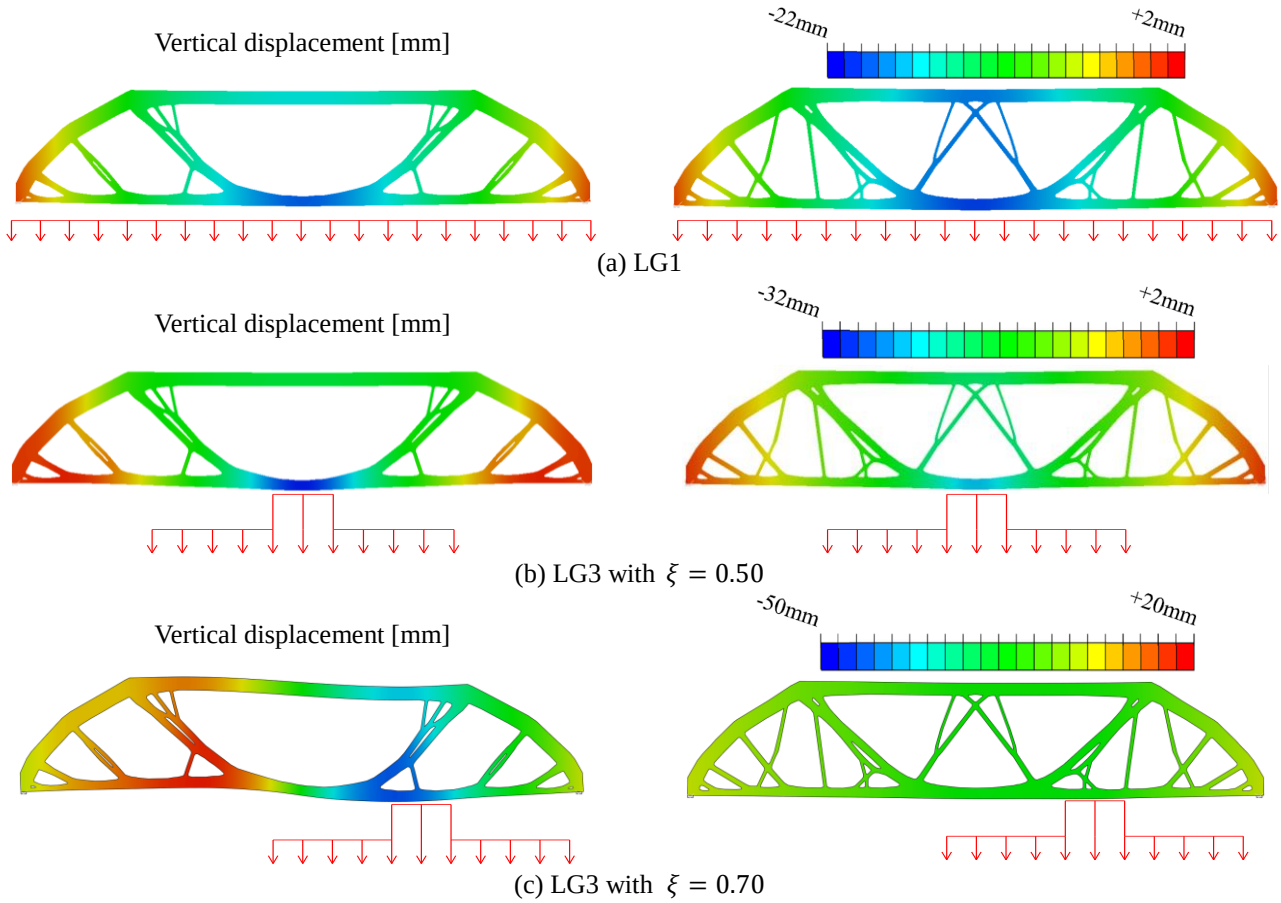

Fig. 12 Contourplots of vertical displacement for different load groups for L50-D10 model (deformation scale factor 20x)

example, a decrease of 20% is found when the convoy is located in the middle of the span, while a 63% decrease is obtained when the convoy is positioned in the first or last quarter of the span. In order to explain the large decline in maximum deflection between a LG3 convoy in the middle and closer to the supports, contourplots of the vertical deformations are depicted in Fig. 12 (b) and (c) for $\xi = 0.50$ and $\xi = 0.70$, respectively. When the LG3 convoy is located in the middle ($\xi = 0.50$), the deformation patterns are quite similar between both topologies, only the magnitude of the deformations of the multiple load topology are systematically marginally smaller than these of the one load topology (See Fig. 12(b)). In contrast, for a LG3 convoy closer to the supports ($\xi = 0.70$), the deformation pattern of the one load topology is very different than for the multiple load topology (See Fig. 12(c)). The load causes the right and left half to displace in downward and upward direction, respectively. This distinct deformation pattern can be attributed to the absence of web members in the middle zone and as a consequence of the lack of shear stiffness in that area.

These results demonstrate that, for this specific case, compliance-volume topology optimization generates better optimized topologies for the strategy under multiple load cases compared to the classical strategies under one or a very limited number of load cases. The main reason of this difference is the consideration of load combinations which load only part of the span (LG3 and LG4). Such loads push the minimal-compliance solution to one with shear stiffness (i.e., web members) over the entire length and as a result reduced (shear) deformations.

As an alternative for topology optimization, which seeks to determine the optimum material distribution within design domain by creating holes such that a certain percentage of the total surface consists of voids, one could also remove material by maintaining the rectangular topology while reducing the initial thickness with the same percentage (i.e., $100 - V^*$ (%)). The ratio of the maximum deflections of both strategies $\delta_{multiple\ load}/\delta_{ref}$ are plotted for convoys LG1 to LG4 in Fig. 11(d) as a function of the relative position of the center of the convoy ξ. In this way, the degree of optimization using a complex topology optimization strategy can be evaluated by comparing the maximum deflections with that obtained from a simple solution where material is uniformly reduced. As expected, it is found from Fig. 11(d) that for this case the maximum deflections of the optimal multi-load topology are smaller (up to 25%) than those from the simple solution.

Next, it is investigated whether the multiple load optimization strategy also yields a different topology for a bridge girder with a depth to span ratio D/L of $1/10$ which is more dominated by pure bending deformation. The second case study has a 50 m span and a depth of 5 m (L50-D05). In Fig. 13, the optimized structures are presented for the different alternatives of topology optimization considering one or multiple load groups LG1 to LG4 (See

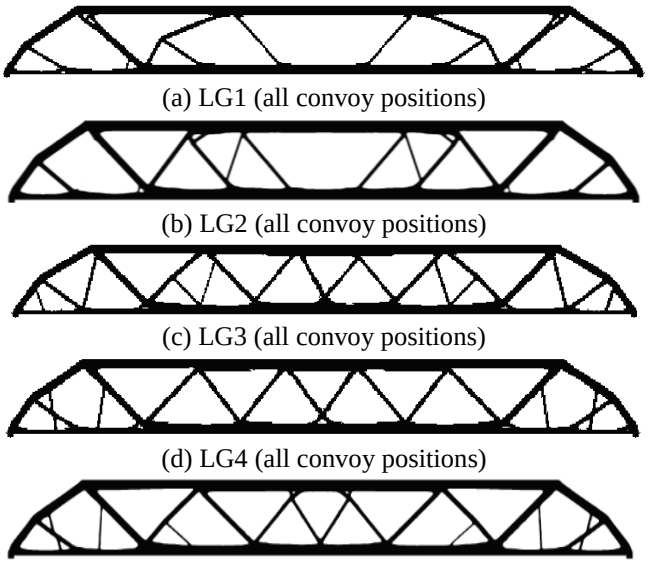

(a) LG1 (all convoy positions)

(b) LG2 (all convoy positions)

(c) LG3 (all convoy positions)

(d) LG4 (all convoy positions)

(e) All load cases and all convoy positions

Fig. 13 Topology optimization results for L50-D05 model optimized for different load groups

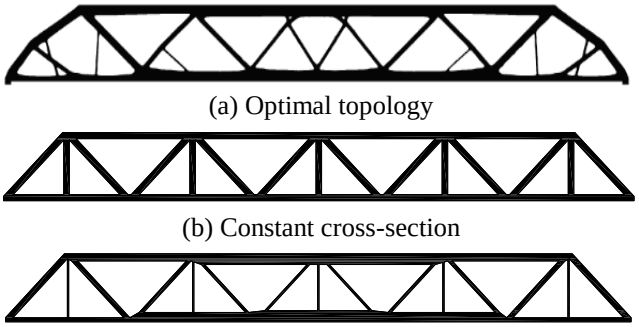

(a) Optimal topology

(b) Constant cross-section

(c) Variable cross-section

Fig. 14 Truss structures for L50-D10 model with a volume fraction V^* of 30% (optimized for all load groups and all convoy positions)

Table 1). For all alternatives, a pure truss structure is found as optimal layout, with the most noticeable difference being the diagonal members. The difference in the number and the location of the diagonals clearly demonstrate the effect of the different load cases on structural topology optimization. Similar to the hybrid topology, a planar truss can be thought of as a beam. The bottom and top chord of the truss have the same function of the flanges of an I-beam and are, respectively, in tension and compression. In contrast to the web of an I-beam, the web of a truss is made of a series of individual members, diagonals and verticals, which have to withstand the shear force. Individually, these members are also in tension or compression. By considering a moving convoy together with a partially loaded span (i.e., LG3 and LG4), the layout is driven to a solution with extra diagonals, which reduce shear deformations (See Fig. 13 (c) to (e)). Again, LG3 and LG4 clearly have a significant impact on the final topology.

To demonstrate the power of topology optimization, the optimal multi-load topology is confronted with two Warren truss structures with verticals (See Fig. 14). For the first

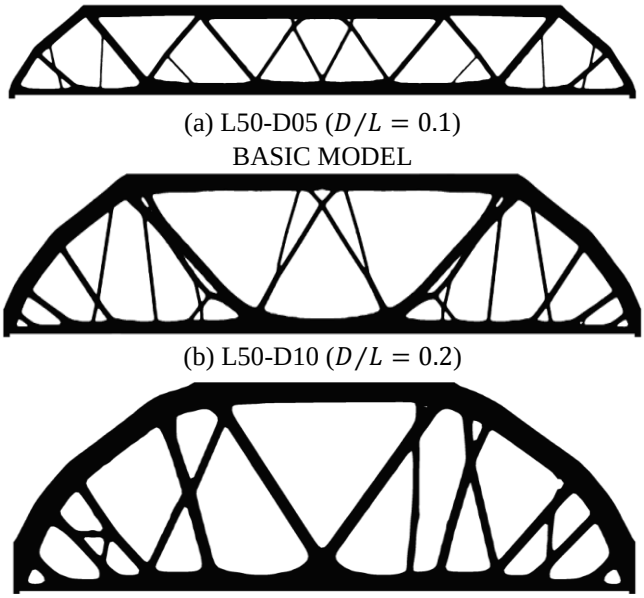

(a) L50-D05 ($D/L = 0.1$)
BASIC MODEL

(b) L50-D10 ($D/L = 0.2$)

(c) L50-D15 ($D/L = 0.3$)

Fig. 15 Optimized topologies for the L50 model with variable depth to span ratio (optimized for all load groups and all convoy positions)

self-designed truss, the 30% material has been uniformly distributed over all members (See Fig. 14(b)). In contrast, all members of the second self-designed truss have a different cross-section. For the truss structure in Fig. 14(c), the material distribution is performed by assigning material to a member according to the maximum force (in absolute value) in that member. These maximum member forces are obtained from envelope curves, which are in turn derived from simple static equilibrium equations for all load cases. In this way, an attempt is made to distribute the material more efficiently. Interestingly, it appears from this confrontation that the maximum deflections of the first and second Warren truss structure are on average, respectively, 44% and 30% larger than for the multi-load topology. In other words, the traditional truss structures are found to be in this case less effective in terms of deformations than the optimized layout.

From these two case studies, it is clear that the layout of the optimized structure strongly depends on the load cases considered during topology optimization. For convenience, topology optimization of structural components is frequently employed using only a simple uniform load. However, as demonstrated here, this strategy does not provide very satisfactory topologies compared to ones obtained with multiple load cases.

5.3 Parametric study for multiple load optimization

In this section, multi-load topology optimization is employed considering all load groups (i.e., LG1 to LG4) and a constant volume fraction V^* of 0.3. In what follows, the depth to span ratio and the support conditions of a one-span bridge will be changed to explore the influence on the topology. Lastly, a two-span bridge is examined.

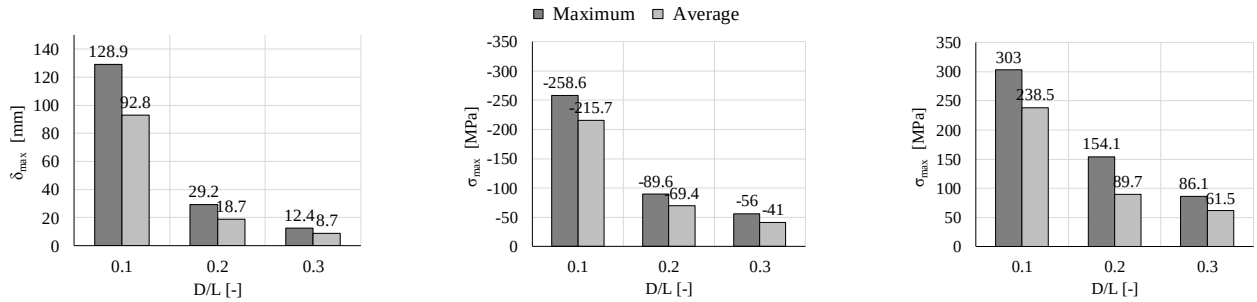

Fig. 16 Maximum and average values (for all load groups and all convoy positions) of the maximum deflection δ_{max} [mm] (left), the maximum compressive stress σ_{max} [MPa] (middle), and maximum tensile stress σ_{max} [MPa] (right) for the L50 model with variable depth to span ratio D/L

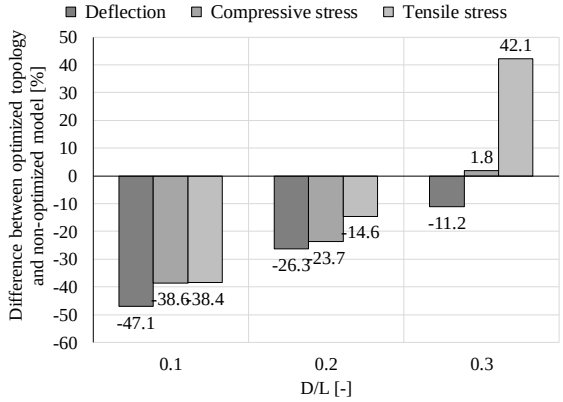

Fig. 17 The average difference (for all load groups and all convoy positions) in percentage of the maximum deflection, compressive and tensile stress between the optimized topology and the non-optimized design domain for the L50 model with variable depth to span ratio D/L

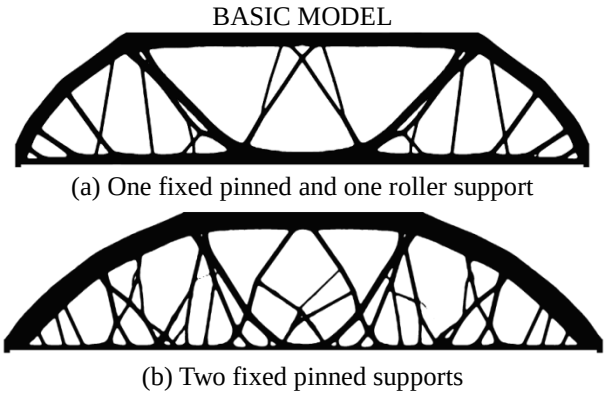

(a) One fixed pinned and one roller support

(b) Two fixed pinned supports

Fig. 18 Topology optimization results for L50-D10 model for a one-span bridge with different support conditions (optimized for all load groups and all convoy positions)

Fig. 19 Viaduc de La Garde-Adhémar (website Bureau Greisch 2016)

5.3.1 Depth to span ratio

Literature provides many different values of the depth to span ratio and the span range for truss and arch structures. Steel truss structures are generally used between 30 m and 150 m, while the truss depth ranges from $1/10$ and $1/15$ of the span. Compared to trusses, arches have larger depth to span ratios. Bridge arches typically have a depth to span ratio between 0.12 to 0.30, and the ideal ratio of a compressed arch is 0.20 (or $1/5$). When the depth of the arch decreases (i.e., a flatter arch), the outward thrust increases and bending becomes dominant, as a result of which the advantageous arch effect (i.e., pure compression) weakens. Nevertheless, in modern slender steel arch bridges due to convoy loading, bending in the arch is inevitable. In addition, arches typically have a span of 50 m and 500 m.

When performing the optimization strategy for a rectangular design domain with a constant length of 50 m and a depth of 5 m ($D/L = 0.1$), 10 m ($D/L = 0.2$), and 15 m ($D/L = 0.3$), the topologies as displayed in Fig. 15 are obtained. Since the volume fraction V^* remains constant, the amount of material - available for the optimization algorithm to distribute over the design domain - increases to the same extent as the increase in depth, thus a doubling (for $D = 10$ m) or a tripling (for $D = 15$ m) compared to the 5 m high model. As expected, the topology evolves with increasing depth to span ratio from a truss structure to a tied hybrid arch-truss bridge.

In Fig. 16, the maximum and average value for all load cases of the maximum deflection, the maximum compressive stress in the top chord/arch, and the maximum tensile stress in the bottom chord/tie are plotted. When the depth to span ratio D/L of the design domain increases, the maximum/average deflection as well as the maximum/ average stresses decrease almost to the same extent.

In Fig. 17, the average difference (in percentage) of the maximum deflection, compressive stress, and tensile stress are given between the optimized topology and the non-optimized rectangular design domain with the same depth to span ratio D/L and the same amount of material by reducing the thickness to 30% of the original thickness.

The first finding is that for all models the average decrease in maximum deflection is larger than the average decrease of maximum stresses, which can be simply explained by the choice of minimization of compliance as objective. Secondly, the average decrease in maximum

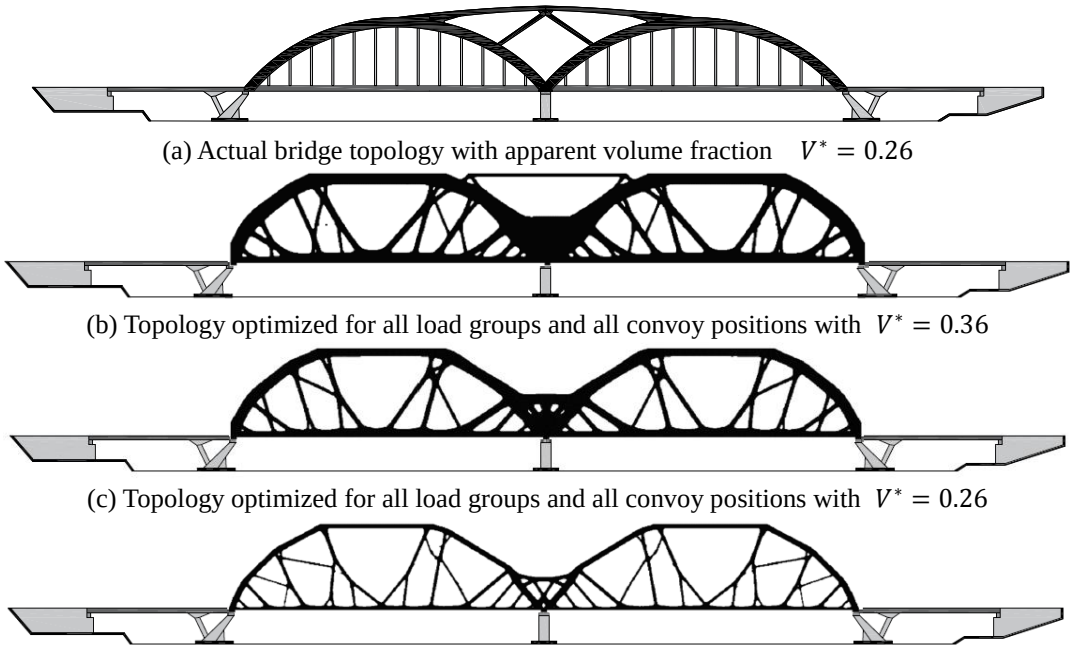

(a) Actual bridge topology with apparent volume fraction $V^* = 0.26$

(b) Topology optimized for all load groups and all convoy positions with $V^* = 0.36$

(c) Topology optimized for all load groups and all convoy positions with $V^* = 0.26$

(d) Topology optimized for all load groups and all convoy positions with $V^* = 0.16$

Fig. 20 Topology of the Viaduc de La Garde-Adhémar

deflections and stresses weakens when the depth to span ratio D/L increases, which indicates that the optimization strategy is more efficient for the truss model than for the higher tied hybrid truss-arch structure. Furthermore, for the highest model (i.e., $D/L = 0.3$), the maximum stresses are actually increasing by applying topology optimization.

5.3.2 Support conditions

For a single-span bridge, the influence of the support conditions on the optimal topology is investigated. The bridge in Fig. 18(a) has one fixed pinned and one roller support, as a result of which the lower chord has to tie the outwardly oriented horizontal forces of the arch, allowing the foundations to be constructed less robust, because the supports only have to absorb the vertical forces. In contrast, two fixed pinned supports of the bridge Fig. 18(b) have to absorb the vertical forces as well as the outward horizontal thrust of the arch. This allows the amount of material in the lower chord to be kept to a minimum. Consequently, topology optimization can distribute more material over the arch and the web members. When comparing both topologies, a few clear differences can be distinguished. The two-fixed supported bridge has a larger arch depth, the arch is less curved over a larger distance, and the horizontal section of the top of the arch is shorter. Furthermore, the lower chord is suspended from the arch by many more hangers distributed along the bridge length.

5.4 Case study: viaduc de la Garde-Adhémar

The viaduct of Garde-Adhémar is a steel tied-arch bridge crossing the Donzère canal and is built for high-speed trains to Southern France (See Fig. 19). The total length of the bridge is about 325 m, which includes two side spans of 52 m each and two main spans of 110.3 m each. The concrete deck of the main spans is suspended from two main arches, which in turn are joined by a central arch above the intermediate support. In plan, the bridge is situated at a skew of approximately 33° relative to the canal. For this case study, the optimization strategy has been applied to demonstrate the applicability of topology optimization for railway bridges.

The elevation view of the real bridge is displayed in Fig. 20(a) and has an apparent volume fraction V^* close to 0.26 (based on the 2D front view), while the optimized topologies with a volume fraction V^* of 0.36, 0.26, and 0.16 are shown in Fig. 20 (b), (c), and (d), respectively. However, it is important to emphasize that the topology optimization here only considered railway load combinations in contrast to the design of the real solution. Nevertheless, a relatively similar design is obtained: a deck which is suspended by hangers on two main arches. There are, of course, also differences between the real and the optimized designs, such as the number and the inclination of the hangers, the amount of material just above the intermediate support, and the central arch. As an alternative to the central arch in the real design, a straight connecting member appears between the main arches for a volume fraction V^* of 0.36. A solution resembling the connection between the tops of the arches is not found.

To study the influence of topology optimization and to assess whether or not the multiple load optimal topology of Fig. 20(c) with the same volume fraction (i.e., $V^* = 0.26$) is in terms of compliance and deformations effectively better than the actual viaduct (depicted in Fig. 20(a)), all topologies are subjected to all loading configurations (LG1 to LG4 with corresponding convoy positions). The compliances and maximum deflections are presented in Fig. 21(a) and Fig. 21(b), respectively. Although the real viaduct has an apparent volume fraction V^* close to 0.26, its

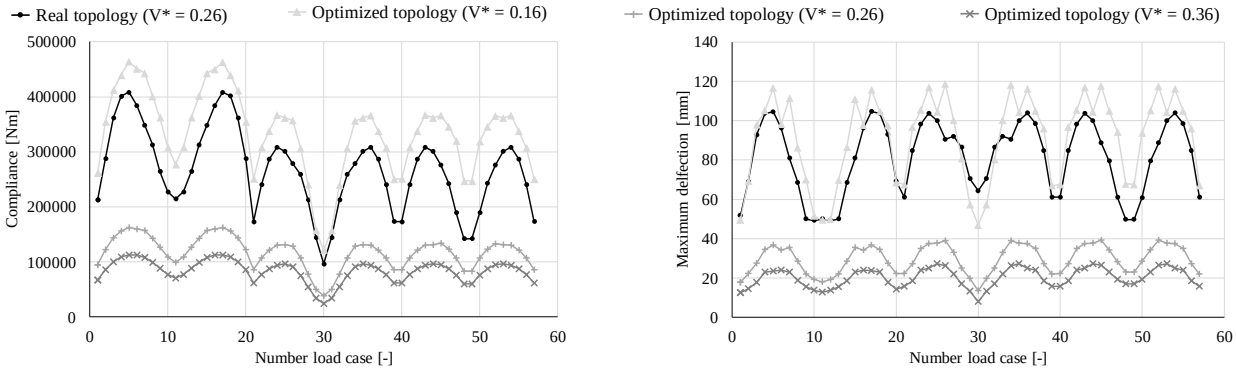

(a) Compliance [Nm] for all load cases (b) Maximum deflection [mm] for all load cases

Fig. 21 Comparison between the real Garde-Adhémar topology and the optimized topologies for the different load cases

compliances and maximum deflections are closest to those of the optimized topology with a volume fraction V^* of 0.16 or thus with a topology with - relatively speaking - 38% less material. Furthermore, it is clear that the optimized topology with the same amount of material (i.e., $V^* = 0.26$) outperforms the actual viaduct for all load groups and all convoy positions. On average, the compliance and the maximum deflection of the optimized topology is, respectively, only 37% and 45% of the actual apparent topology.

6. Conclusions

The SIMP formulation with the minimization of compliance as objective and a volume constraint have been used as optimization strategy for steel railway bridges, while taking into account multiple loads configurations. This multiple load topology optimization strategy presented in this work gives a structural engineer a valuable alternative to quickly identify an optimal layout. Using commercial available FE analyses, fascinating topologies can be designed which are excellent in terms of structural efficiency (i.e., deformations) and are in the meanwhile esthetically pleasing. In summary, the main contributions of this work are as follows:

- The relevance of considering multiple load conditions, such as moving convoys and partially loaded spans, during topology optimization has been demonstrated.
- Compared to the classical strategy, considering only one or a limited number of load cases, a substantially different optimal layout is obtained which in addition exhibits smaller deformations for most load cases.
- The influence of the volume fraction, the depth to span ratio, and the support conditions have been illustrated.
- As case study topology optimization has been applied to the viaduct de la Garde-Adhémar. By comparing the compliances and the deflections between the optimized topologies and the apparent actual bridge geometry, it has been demonstrated that topology optimization could substantially improve the performance compared to a classic layout. On average the optimized topology has a maximum deflection which is 45% of the non-optimized apparent viaduct geometry with the same amount of material.

To conclude, topology optimization is successful in finding structures where at the same time the material is optimized and the weight reduced, enhancing the structural efficiency, and therefore we strongly believe topology optimization will become an appreciated tool for attacking structural and civil engineering problems, including bridge design.

Acknowledgments

The authors are very grateful to Jesse Houf and Josse Billiau for participating in this study.

References

Beghini, L.L., Beghini, A., Katz, N., Baker, W.F. and Paulino, G.H. (2014), "Connecting architecture and engineering through structural topology optimization", *Eng. Struct.*, **59**, 716-726.

Bendsøe, M.P. (1989), "Optimal shape design as a material distribution problem", *Struct. Optim.*, **1**(4), 193-202.

Bendsøe, M.P. and Sigmund, O. (2003), *Topology Optimization: Theory, Methods and Applications*, Springer-Verlag, Berlin Heidelberg, New York, NY, USA.

Briseghella, B., Fenu, L., Lan, C., Mazzarolo, E. and Zordan, T. (2013), "Application of topological optimization to bridge design", *J. Bridge Eng.*, **18**(8), 790-800.

Briseghella, B., Fenu, L., Yeng, Y., Lan, C., Mazzorolo, E. and Zordan, T. (2016), "Optimization indexes to identify the optimal design solution of shell-supported bridges", *J. Bridge Eng.*, **21**(3), 04015067.

CEN (2003), Eurocode 1: Actions on structures - Part 2: Traffic loads on bridges, European Committee for Standardization, Brussels, Belgium.

CEN (2006), Eurocode 3: Design of steel structures - Part 2: Steel bridges, European Committee for Standardization, Brussels, Belgium.

Fauche, E., Adriaenssens, S. and Prevost, J.H. (2010), "Structural optimization of a thin-shell bridge structure", *J. IASS*, **51**(2), 153-160.

Huang, X. and Xie, Y.M. (2008), "Optimal design of periodic structures using evolutionary topology optimization", *Struct. Multidiscip. O.*, **36**(6), 597-606.

Iwamura, R.S. and de Faria, A.R. (2013), "Topology optimization

of multiple load case structures", *Proceedings of International Symposium on Solid Mechanics*, Porte Alegre, Brazil, April.
Kutylowski, R. and Rasiak, B. (2014a), "Application of topology optimization to bridge girder design", *Struct. Eng. Mech.*, **51**(1), 39-66.
Kutylowski, R. and Rasiak, B. (2014b), "The use of topology optimization in the design of truss and frame bridge girders", *Struct. Eng. Mech*., **51**(1), 67-88.
Liu, S. and Qiao, H. (2011), "Topology optimization of continuum structures with different tensile and compressive properties in bridge layout design", *Struct. Multidiscip O*., **43**(3), 369-380.
Luo, Y. and Kang, Z. (2012), "Topology optimization of continuum structures with Drucker-Prager yield stress constraints", *Comput. Struct*., **90**, 65-75.
Rahmatalla, S. and Swan, C.C. (2003), "Form finding of sparse structures with continuum topology optimization", *J. Struct. Eng*., ASCE, **129**(12), 1707-1716.
Rozvany, G.I.N. and Birker, T. (1994), "On singular topologies in exact layout optimization", *Struct. Optim*., **8**(4), 228-235.
Simulia (2014a), ABAQUS 6.14 (computer software) Dassault Systèmes Simulia Corp., Providence, RI, USA.
Simulia (2014b), Tosca Structure (computer software) Dassault Systèmes Simulia Corp., Providence, RI, USA.
Stromberg, L.L., Beghini, A., Baker, W.F. and Paulino, G.H. (2012), "Topology optimization for braced frames: Combining continuum and beam/column elements", *Eng. Struct*., **37**, 106-124.
Tang, J., Xie, Y.M. and Felicetti, P. (2014), "Conceptual design of buildings subjected to wind load by using topology optimization", *Wind Struct*., **18**(1), 21-35.
Viaduc de La Garde-Adhémar, Bureau Greisch, www.greisch.com/projet/viaduc_donzere_mondragon, Accessed 18 November 2016.
Yang, R.J. and Chuang, C.H. (1994), "Optimal topology design using linear programming", *Comput. Struct*., **52**(2), 265-275.
Zuo, Z.H., Huang, X., Black, T. and Felicetti, P. (2014), "Application of topological optimisation technology to bridge design", *Struct. Eng. Int*., **24**(2), 185-191.
Zuo, Z.H., Xie, Y.M. and Huang, X. (2012), "Evolutionary topology optimization of structures with multiple displacement and frequency constraints", *Adv. Struct. Eng*., **15**(2), 359-372.

CC